

Supporting Information for

Concave Trisoctahedral Ag_3PO_4 Microcrystals with High-index Facets and Enhanced Photocatalytic Properties

Zhengbo Jiao,[†] Yan Zhang,[†] Hongchao Yu,[†] Gongxuan Lu,[†] Jinhua Ye,[‡] and Yingpu Bi^{†,*}

[†] State Key Laboratory for Oxo Synthesis & Selective Oxidation (OSSO), and National Engineering Research Center for Fine Petrochemical Intermediates (NERC-FPI), Lanzhou Institute of Chemical Physics, CAS, Lanzhou 730000, China.

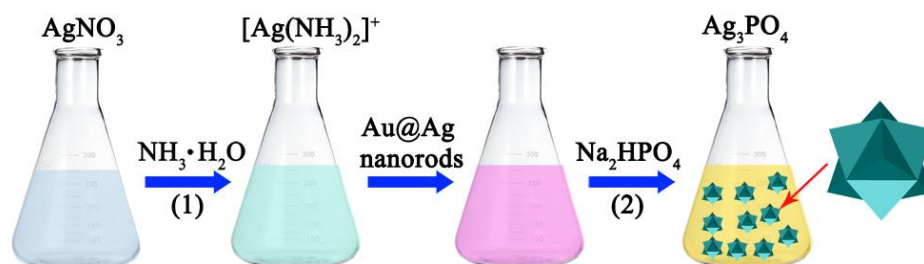
[‡] International Center for Materials Nanoarchitectonics (MANA), and Research Unit for Environmental Remediation Materials, National Institute for Materials Science (NIMS), Tsukuba, 305-0047, Japan

*To whom correspondence should be addressed.

Email: yingpubi@licp.cas.cn

Experimental Section

1. Synthesis of TOH Ag_3PO_4



Scheme S1. Schematic illustration of the growth process of TOH Ag_3PO_4 microcrystals when Au@Ag nanorods with high aspect ratio are used as seeds.

(1) Preparation of Au@Ag nanorods with high aspect ratio

Firstly, the Au nanorods with high aspect ratio were synthesized by the method described by C. J. Murphy et al. with minor modification.[1] In general, Au nanorods with high aspect ratio were prepared by two steps. In the first step, 4 nm gold nanoparticles were produced by the reduction of HAuCl_4 (250 μl , 10 mM) with sodium borohydride (0.6 ml, 10 mM) in the presence of cetyltrimethylammonium bromide (CTAB) (7.5 ml, 0.1M). In the second step, 4 nm gold nanoparticles (10 μl) were added to the growth solution containing CTAB (5 ml, 0.1M), HAuCl_4 (200 μl , 10 mM) and ascorbic acid (AA) (32 μl , 0.1M). The gold nanorods were collected by centrifugation and washed three times. Besides Au nanorods with high aspect ratio, Au nanorods

with low aspect ratio and trepan-like Au nanorods could be prepared with the similar procedure except under the existence of silver nitrate during the growth and overgrowth of Au nanorods with high aspect ratio, respectively. Silver nanowires could be synthesized through the reduction of silver nitrate by 1,3-butylene glycol in PVP solution which have been reported by us recently.[2]

Secondly, the Au@Ag nanorods with high aspect ratio were produced by the method reported by P. Guyot-Sionnest et al. with minor modification.[3] For the traditional synthesis of Au@Ag nanocrystals, 1 ml gold nanorods (0.5 mM) were added into 4ml PVP ($M_w \approx 10000$) aqueous solution (1 wt%) under stirring. To this solution, 80 μ l AgNO_3 (10 mM), 100 μ l AA (0.1M) and 200 μ l NaOH (0.1 M) were then added. The reaction was finished in about 20 min and the solution was centrifuged twice before used as seeds.

(2) Preparation of TOH Ag_3PO_4 microcrystals

The TOH Ag_3PO_4 crystals were prepared by a simple precipitation process (shown in Scheme S1). In a typical synthesis, AgNO_3 (0.2g) was solved in aqueous solution. Ammonia aqueous solution (0.1M) was added with drop by drop to the above solution to form a transparent solution. Then the Au@Ag nanorods with high aspect ratio which were used seeds and Na_2HPO_4 aqueous solution (0.15M) were added in order. The olivine TOH Ag_3PO_4 crystals have been synthesized.

2. Photocatalytic Reactions

In all catalytic activity of experiments, the samples (0.2g) were put into a solution of RhB dyes (100ml, 8mg/L), which was then irradiated with a 300 W Xe arc lamp equipped with an ultraviolet cutoff filter to provide visible light with $\lambda \geq 420$ nm. The degradation of organic dyes was monitored by UV/Vis spectroscopy (UV-2550PC, Shimadzu). The photocatalysts were removed from the photocatalytic reaction systems by a dialyzer before the spectroscopy measurement.

3. Characterization

The morphology and size of the as-prepared product were characterized by using a field-emission scanning electron microscope (JSM-6701F, JEOL) operated at an accelerating voltage of 5 kV. The X-ray diffraction spectra (XRD) measurements were performed on a Rigaku RINT-2000 instrument using $\text{Cu K}\alpha$ radiation (40 kV). The XRD patterns were recorded from 10° to 90° with a scanning rate of 0.067 $^\circ/\text{s}$. UV-vis diffuse reflectance spectra were taken on a UV-2550 (Shimadzu) spectrometer by using BaSO_4 as the reference. The element composition was detected by X-ray photoelectron spectroscopy (XPS, Kratos Axis Ultra DLD).

4. Calculations

The first-principles calculations were performed within the local-density approximation (LDA) framework, as implemented in the CASTEP module [4,5] of Materials Studio 5.5. The used exchange-correlation functional is CA-PZ, which is proposed by Ceperley and Alder [6] and parameterized by Perdew and Zunger [7]. The ultrasoft pseudopotential is adopted to deal with the interaction between ion cores and valence electrons. The valence electron configurations of the ultrasoft pseudopotentials for Ag, P, and O are $4d^{10}5s^1$, $3s^23p^3$, and $2s^22p^4$, respectively. For the 16-atom Ag_3PO_4 unit cell (space group $P\bar{4}3n$), the Monkhorst-Pack k -point set of $4\times 4\times 4$ was used for Brillouin Zone sampling. The cutoff energy of plane-wave basis set was taken to be 400 eV. Geometry optimization was performed by the BFGS algorithm under convergence tolerances of 2.0×10^{-5} eV/atom for energy, 0.05 eV/Å for maximum force, 0.002 Å for maximum displacement, 0.1 GPa for maximum stress. The self-consistent field electronic minimization was carried out with a convergence threshold of 2.0×10^{-6} eV/atom. On the basis of LDA optimized structures, we performed single point energy calculations using the LDA+ U approach with $U_d(\text{Ag})$ of 7.2 eV, $U_p(\text{P})$ and $U_p(\text{O})$ of 7.0 eV according to Zhu and coworkers [8].

The optimized cell parameters are $a=b=c=5.864$ Å, which is a little lower than the experimental value of 6.004 Å [9]. The calculated Ag-O and P-O bond lengths are 2.307 and 1.528 Å, respectively, which agree with the experimental data of 2.345 and 1.539 Å [9], the previous LDA results of 2.314, 1.529 Å [8] and 2.31, 1.55 Å [10], and the PBE0 results of 2.386, 1.518 Å [11]. As presented in Figure S1, the calculated indirect bandgap is 2.406 eV, which agrees with the experimental bandgap of 2.36 eV [12].

For modelling the surface, the 96-atom Ag_3PO_4 slab was cleaved from the optimized cell above. The position of cleavage was carefully selected to reduce the dipole moment induced by two asymmetric surfaces of the slab. The vacuum slab of 15 Å was added to eliminate the interaction between slabs due to the periodic boundary conditions. The middle 32 atoms were fixed to mimic the ideal Ag_3PO_4 bulk crystal, leaving the remaining 32 atoms of each surface relaxed.

The surface energy was calculated by

$$\gamma = \frac{E_{slab} - nE_{bulk}}{2A},$$

where E_{slab} is the total energy of the slab, E_{bulk} is the total energy per bulk unit cell, n is the

number of bulk unit cells included in the slab, and A is the surface area of each side of the slab.

The obtained surface energies of (100), (221) and (332) are 1.02, 2.01 and 1.41 J/m², respectively. We also calculated the (110) surface of Ag₃PO₄. The surface energy is 1.12 J/m², higher than that of (100) surface, which gives similar results to the previous LDA+ U calculations [13].

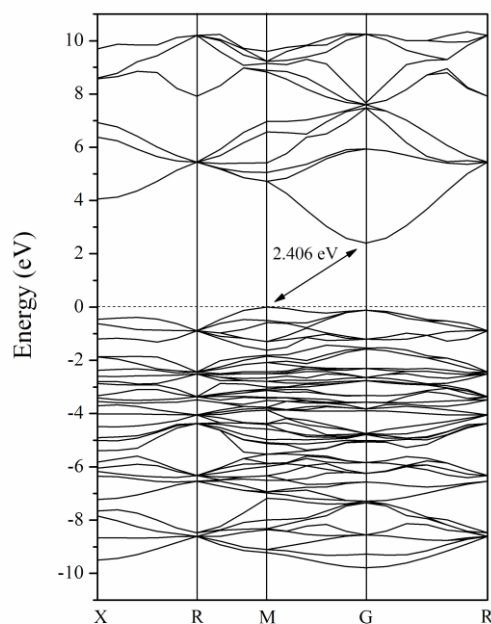


Fig. S1. Energy band structure of Ag₃PO₄ calculated by the LDA+ U method.

References

- [1] B. D. Busbee, S. O. Obare, C. J. Murphy, *Adv. Mater.* **2003**, *15*, 414.
- [2] Y. Bi, J. Ye, *Chem. Commun.* **2009**, 6551.
- [3] M. Liu, P. Guyot-Sionnest, *J. Phys. Chem. B* **2004**, *108*, 5882.
- [4] M. D. Segall, P. J. D. Lindan, M. J. Probert, C. J. Pickard, P. J. Hasnip, S. J. Clark, M. C. Payne, *J. Phys.: Condens. Matter* **2002**, *14*, 2717.
- [5] S. J. Clark, M. D. Segall, C. J. Pickard, P. J. Hasnip, M. J. Probert, K. Refson, M. C. Payne, *M. C. Z. Kristallogr.* **2005**, 220, 567.
- [6] D. M. Ceperley, B. J. Alder, *Phys. Rev. Lett.* **1980**, *45*, 566.
- [7] J. P. Perdew, A. Zunger, *Phys. Rev. B* **1981**, *23*, 5048.
- [8] X. G. Ma, B. Lu, D. Li, R. Shi, C. S. Pan, Y. F. Zhu, *J. Phys. Chem. C* **2011**, *115*, 4680.
- [9] H. N. Ng, C. Calvo, R. Faggiani, *Acta Crystallogr. B* **1978**, *34*, 898.
- [10] N. Umezawa, S. X. Ouyang, J. H. Ye, *Phys. Rev. B* **2011**, *83*, 035202.
- [11] J. J. Liu, X. L. Fu, S. F. Chen, Y. F. Zhu, *Appl. Phys. Lett.* **2011**, *99*, 191903.
- [12] Z. G. Yi, J. H. Ye, N. Kikugawa, T. Kako, S. X. Ouyang, H. Stuart-Williams, H. Yang, J. Y. Cao, W. J. Luo, Z. S. Li, Y. Liu, R. L. Withers, *Nat. Mater.* **2010**, *9*, 599.
- [13] Y. P. Bi, S. X. Ouyang, N. Umezawa, J. Y. Cao, J. H. Ye, *J. Am. Chem. Soc.* **2011**, *133*, 6490.

Additional Figures and Discussions

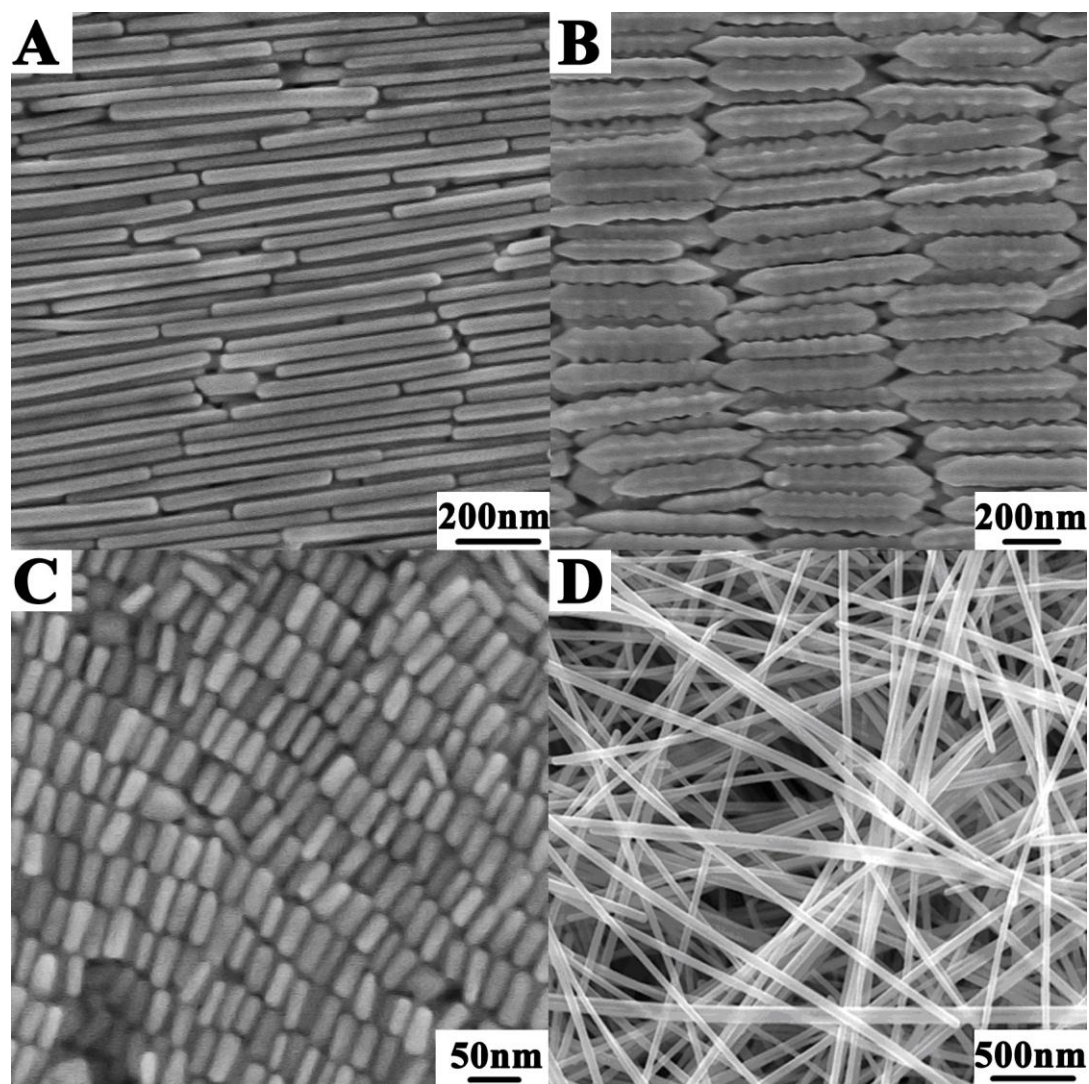


Fig. S2. SEM images of (A) Au@Ag nanorods with high aspect ratio, (B) trepang-like Au@Ag nanorods, (C) Au@Ag nanorods with short aspect ratio, and (D) Ag nanowires, which were used as seeds in the preparation of TOH, TOH with obtuse boundary, tetrahedral, and necklace-like Ag_3PO_4 , respectively.

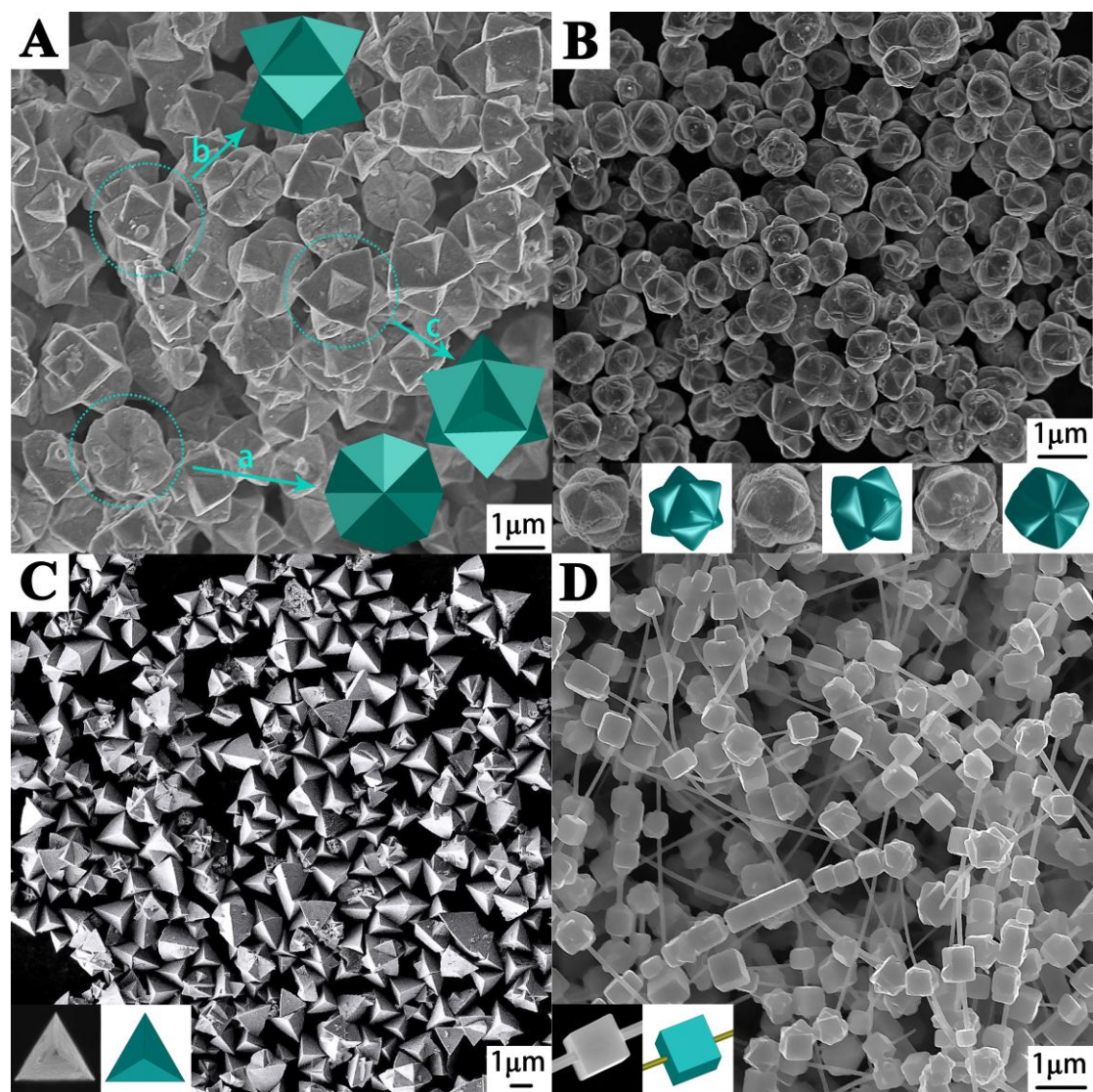


Fig. S3. SEM images of (A) TOH, (B) TOH with obtuse boundary, (C) tetrahedral, and (D) necklace-like Ag_3PO_4 and the insets are single SEM image and corresponding model of them. Among them, the three model in (A) are viewed along (a) $\langle 100 \rangle$, (b) $\langle 110 \rangle$ and (c) $\langle 111 \rangle$ crystallographic direction, respectively.

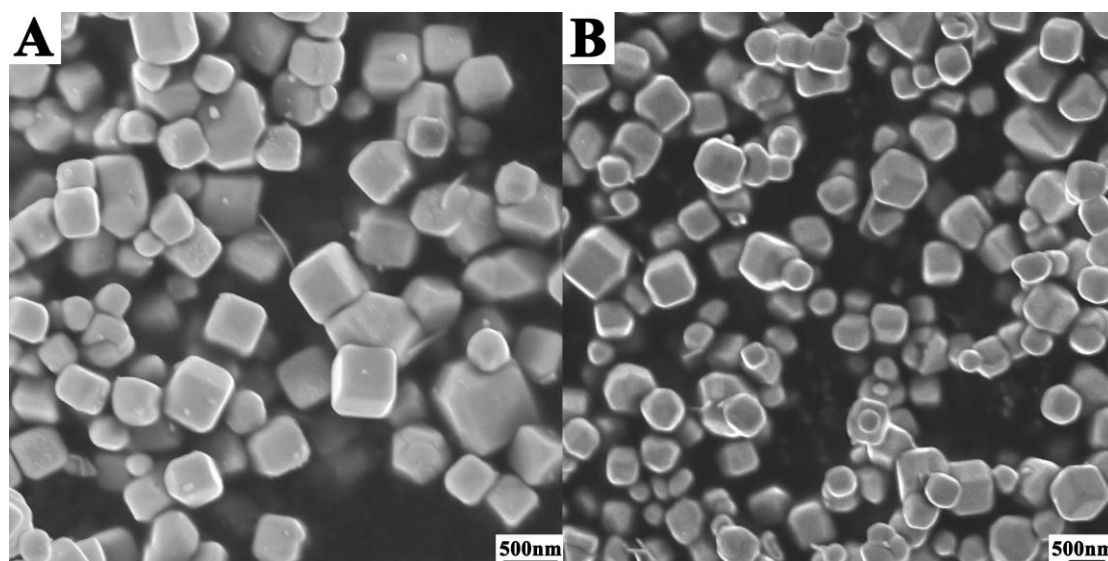


Fig. S4. SEM images of Ag_3PO_4 products which were synthesized by reacting $[\text{Ag}(\text{NH}_3)_2]^+$ with (A) NaH_2PO_4 and (B) H_3PO_4 .

Results and discussion

It should be noted that Na_2HPO_4 play a crucial role in the successful preparation of TOH Ag_3PO_4 microcrystals. As shown in Fig. S4A,B when Na_2HPO_4 was replaced by NaH_2PO_4 or H_3PO_4 , only the mixture of irregular cubic Ag_3PO_4 crystals and Au@Ag nanorods were obtained, and no any TOH Ag_3PO_4 was formed. On the basis of above results, we consider that TOH morphology could only be formed with a suitable release rate Ag^+ ions from $[\text{Ag}(\text{NH}_3)_2]^+$ complex. More specifically, the rapid release rate of Ag^+ ions from $[\text{Ag}(\text{NH}_3)_2]^+$ complex as a result of the more H^+ ions contained in NaH_2PO_4 and H_3PO_4 should be disadvantage for the selectively epitaxial growth of TOH Ag_3PO_4 microcrystals on the Au@Ag nanorods.

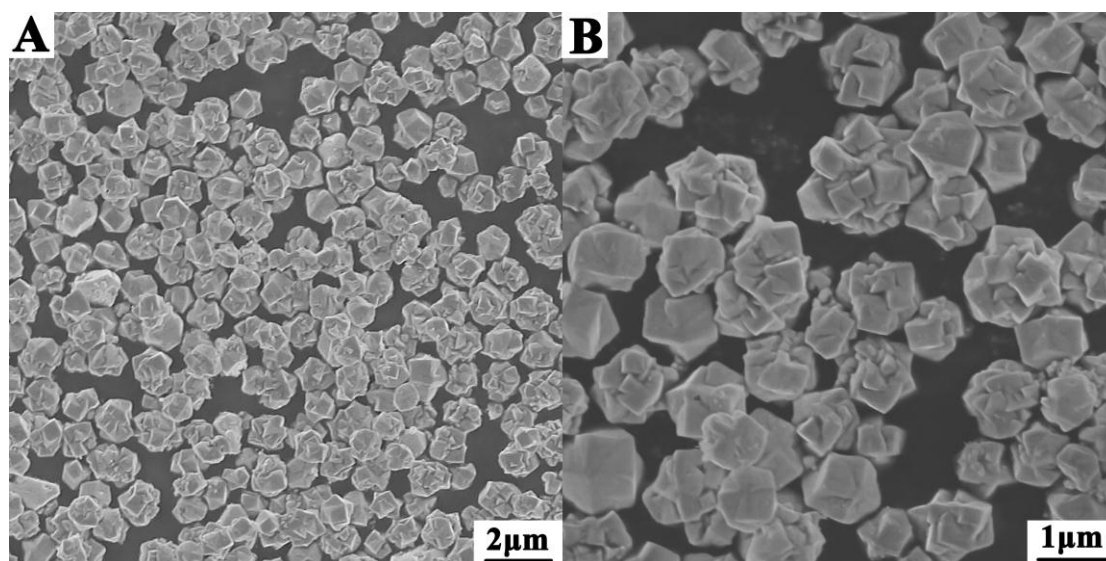


Fig. S5. SEM images of Ag_3PO_4 products with different magnifications when Au nanorods with high aspect ratio were used as seeds directly.

Results and discussion

As shown in Fig. S5, when pure Au nanorods were used as the growth template, TOH Ag_3PO_4 could not be obtained. Herein, we consider that it is necessary to coat a thin nanofilm of silver on the surface of gold nanorods for the successful preparation of Ag_3PO_4 with TOH morphology. Furthermore, the Ag^+ may be easily adsorbed on the Ag atom, which may facilitate the heteroepitaxial growth of Ag_3PO_4 outside of Au@Ag nanorods.

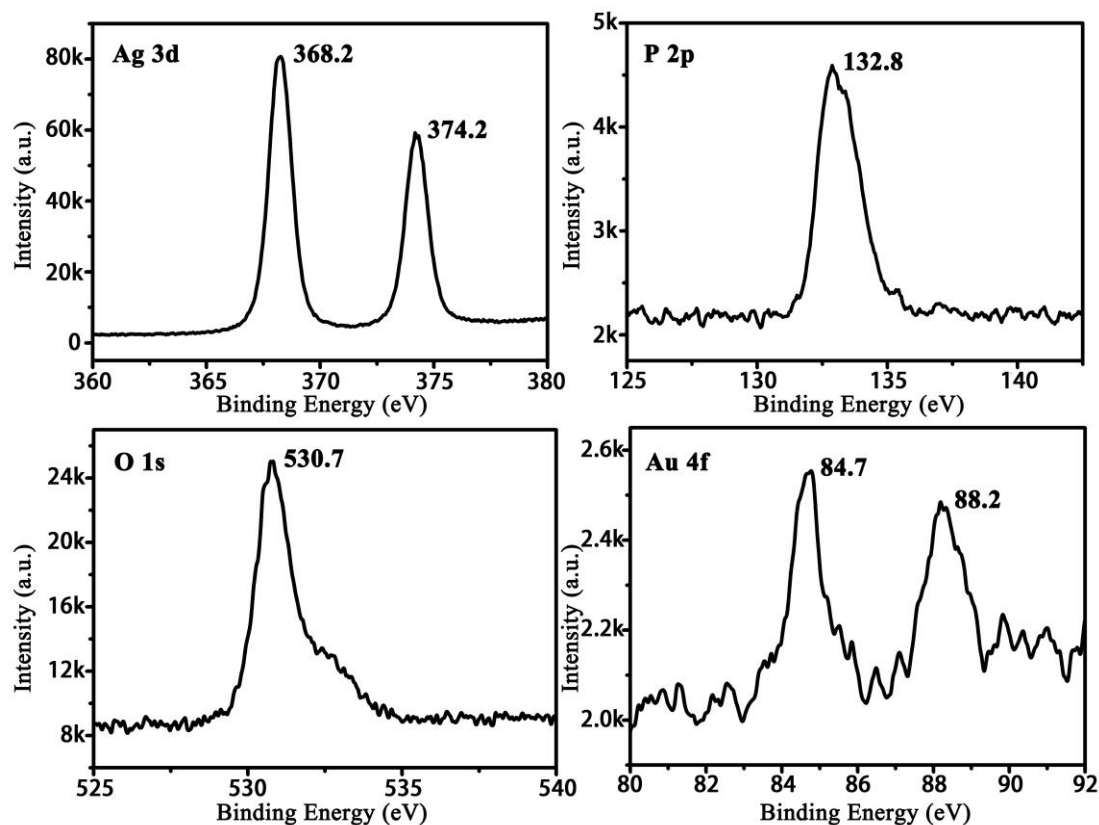


Fig. S6. High resolution XPS spectra of the as-prepared TOH Ag₃PO₄: (A) Ag 3d, (B) P 2p, (C) O 1s and (D) Au 4f.

Results and discussion

It can be seen from the above XPS results that the binding energy at 368.2 and 374.2 eV can be attributed to 3d_{5/2} and 3d_{3/2} of silver.¹ Furthermore, the P 2p peak at 132.8 eV and O 1s peak at 530.7 eV can be indexed to P⁵⁺ cation and O²⁻ anion, respectively.² The doublet at 84.7 eV and 88.2 eV can be attributed to 4f_{7/2} and 4f_{5/2} of gold. These values are slightly higher than the corresponding binding energy of Au⁰ but lower than that of ionic states of gold, which may due to the formation of bimetallic Ag/Au on their hetero-interface.³

References

- [1] H. Zhang, G. Wang, D. Chen, X. J. Lv, J. H. Li, *Chem. Mater.* **2008**, *20*, 6543.
- [2] a) R. Y. Zheng, L. Lin, J. L. Xie, Y. Z. Zhu, Y. C. Xie, *J. Phys. Chem. C.* **2008**, *112*, 15502; b) H. Yang, X. L. Wu, M. H. Cao, Y. G. Guo, *J. Phys. Chem. C.* **2009**, *113*, 3345.
- [3] a) C. D. Wagner, W. M. Riggs, L. E. Davis, J. F. Moulder, G. E. Muilenberg, "Handbook of X-Ray Photoelectron Spectroscopy" Physical Electronics, Eden Prairie, **1979**, 154; b) Briggs D.; Seah M. P. Practical surface analysis. London: J. Wiley & Sons **1996**, 533. c) S. W. Han, Y. Kim, K. Kim, *J. Colloid Interface Sci.* **1998**, *208*, 272.

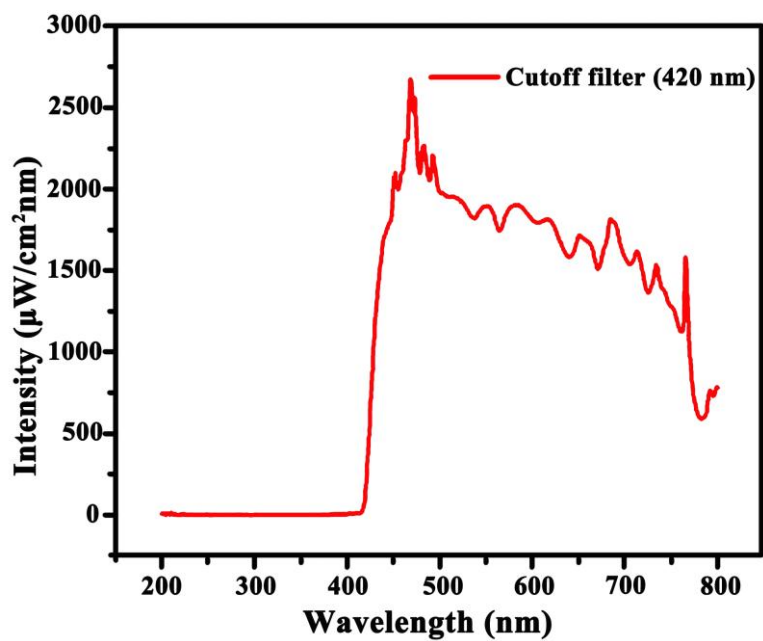


Fig. S7. The intensity and wavelength distribution of the irradiation light employed in the organic decomposition experiments. Integral intensities were measured under the actual experimental conditions.

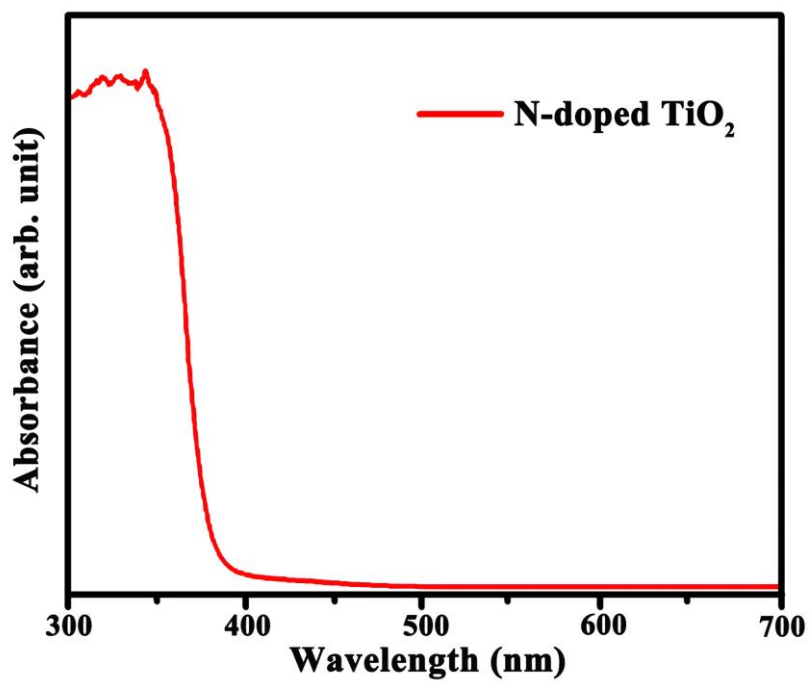


Fig. S8. The ultraviolet–visible diffusive reflectance spectrum of N-doped TiO₂.

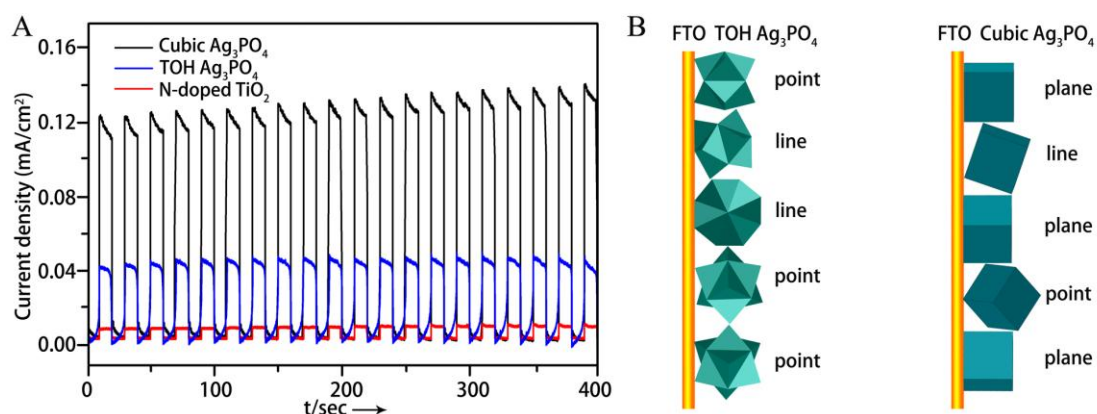


Fig. S9. (A) Photoelectric conversion performances of cubic Ag₃PO₄, TOH Ag₃PO₄, and N-doped TiO₂ in 0.1 M Na₂SO₄ aqueous solutions under visible light irradiation. (B) Schematic illustration of TOH Ag₃PO₄ and cubic Ag₃PO₄ arrays on the FTO glass.

Results and discussion

It is well known that semiconductors exhibit unique photoelectric properties owing to their intrinsic band gap structure, which provides a simple and economical light-to-electric conversion approach for various energy-related applications. The photoelectric conversion properties over TOH Ag₃PO₄ deposited on Fluorine doped tin oxide (FTO) glass have been investigated in detail (Fig. S9A). It can be found that the photoelectric current of TOH Ag₃PO₄ is higher than N-doped TiO₂ but lower than cubic Ag₃PO₄. The schematic illustration of TOH Ag₃PO₄ and cubic Ag₃PO₄ arrays on the FTO glass have been shown in Fig. S9B. Due to the inherent characteristic of TOH morphology, it can be found that the contact area between TOH Ag₃PO₄ and FTO glass is much smaller than that of cubic Ag₃PO₄, which should be not beneficial for the separation and transport of photoexcited electron-hole pairs. As for cubic Ag₃PO₄, most of them contact the FTO glass effectively through their flat {100} planes, which result in the fast separation of photoexcited electron-hole pairs and therefore exhibit the highest photoelectric conversion properties.

| {hkl} \ Angel | α | β | γ |
|---------------|----------|---------|----------|
| {221} | 141° | 90° | 141° |
| {331} | 129.5° | 102° | 153.5° |
| {441} | 124° | 108° | 160° |
| {332} | 153.5° | 78° | 129.5° |
| {553} | 148.5° | 83° | 134° |

Table S1. The calculated values for the the angels α , β and γ when the TOH is bounded by different crystallographic facets.